Dynamic Stability of Flexible Forward Swept Wing Aircraft

Terrence A. Weisshaar* and Thomas A. Zeiler†
Purdue University, West Lafayette, Indiana

This paper discusses the importance of including aircraft rigid-body modes in the aeroelastic analysis of forward swept wing aircraft. Several examples are used to show that body-freedom flutter and aircraft aeroelastic divergence, not wing divergence, are the primary vehicle aeroelastic instabilities to be encountered by forward swept wing aircraft. These instabilities are shown to occur close to the wing divergence speed, but depend upon the aircraft geometry and inertial characteristics as well as wing stiffness.

Introduction

Requirements for high-speed aircraft performance demand that close attention be given to the aeroelastic stability of the vehicle. Aerodynamic loads caused by the interaction between aircraft rigid-body motion and structural flexibility may be particularly important to the correct determination of vehicle instabilities. Forward swept wing (FSW) technology[1,2] has provided added impetus to study the potential interaction between vehicle flexibility and traditional rigid-body flight mechanics. When an FSW is cantilevered at its root, an aeroelastic instability called "wing divergence" may appear; this instability is characterized by a loss of effective wing stiffness. However, for the free-flight condition, wing root fixity is no longer present. Because of this, serious questions have been raised about the applicability of wing divergence calculations to a freely flying aircraft.

Miller et al.[3] discovered the potential for interaction among rigid body pitch and plunge and the flexible modes of a proposed FSW demonstrator aircraft. They showed that this interaction could produce a dynamic instability at speeds lower than the wing divergence speed. Wing divergence did not appear as an instability in any of their analyses. A similar aeroelastic phenomenon was also identified by Weisshaar[4] during the analysis of a small wind tunnel model. The Air Force Flight Dynamics Laboratory conducted a series of low-speed wind tunnel tests to examine the potential for this unusual type of vehicle instability.[5] These tests confirmed that, under certain circumstances, wing divergence was not the true mode of FSW aeroelastic instability. Instead, a phenomenon termed "body-freedom flutter" appeared as a possible mode of vehicle instability. These previous studies have raised a number of issues that this paper will attempt to illuminate. To achieve this objective, the simplest possible idealized model was chosen for vehicle stability studies. It is to this model and these studies that attention now turns.

A Free-Free FSW Aeroelastic Model

It is well recognized that one may modify the calculated flutter speed of a cantilevered wing by including the free-free or zero-frequency modes of the aircraft. The earliest report on the subject of the influence of "body freedom" on flutter is due to Frazer and Duncan.[6] A number of other papers and reports discuss the potential for producing a dynamic instability by coupling together flexible modes with body-freedom modes such as the short-period mode or the roll mode.[7-5]

The cited references on body-freedom flutter discuss the essential features of an analytical model for aeroelastic studies of this type. First of all, the reduced frequency (as opposed to the actual oscillatory frequency) of the unstable oscillation is usually low enough to allow the use of quasi-steady aerodynamics in the model and still obtain meaningful results. While some inaccuracies may arise from the exclusion of aerodynamic lag terms, the demonstration of the phenomenon is greatly simplified by their absence. For this reason, quasi-steady aerodynamic theory (including the damping terms) was chosen for the present model.

A minimum of three degrees-of-freedom are necessary for the vehicle stability model. Wing bending flexibility is the primary source of FSW wing divergence and is therefore part of the trigger mechanism for flexible aircraft instability. Fuselage pitch attitude is also important because it is associated with the so-called short-period mode of the aircraft. The frequency of the pitch mode tends to increase with airspeed while, in contrast, the wing bending frequency decreases with airspeed, creating the potential for a classical frequency coalescence instability. Finally, the plunge velocity creates aerodynamic damping that is important to the coupled motion of the aircraft and, in turn, its stability.

An illustration of the idealized model degrees-of-freedom used in the present study is shown in Fig. 1. A planform view of this three-degree-of-a-freedom model appears in Fig. 2. The airplane idealization has a rigid canard/tail surface included. As shown in Fig. 2, this stabilizer surface has a center of pressure located a distance d ahead of the aircraft center of gravity. This parameter, d, is less than zero when the surface is located aft of the aircraft c.g., making it a tail surface. No

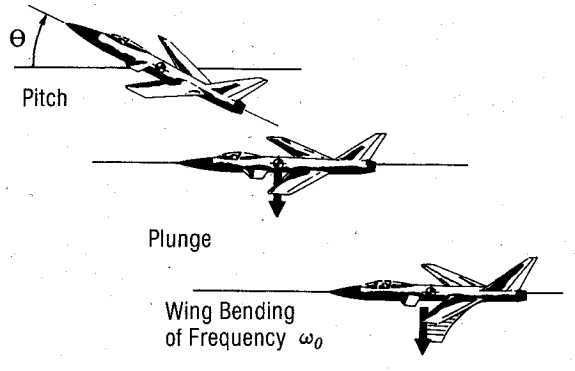

Fig. 1 Aircraft degrees-of-freedom

Presented as Paper 82-1325 at the AIAA Ninth Atmospheric Flight Mechanics Conference, San Diego, Calif., Aug. 9-11, 1982; received Aug. 9, 1982; revision received April 19, 1983.

*Professor, School of Aeronautics and Astronautics. Member AIAA.

†Research Assistant. Member AIAA.

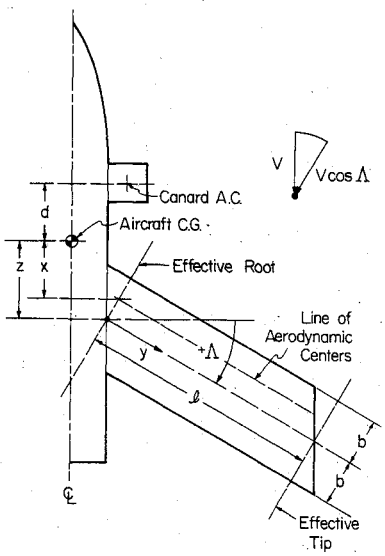

Fig. 2 Planform geometry and dimensions of the aircraft model.

attempt was made to account for aerodynamic interference between the canard/tail and the wing. A distance x denotes the distance between the aircraft c.g. and intersection of the wing quarter-chord line with the effective wing root. This distance, divided by wing semi-span l, appears as $\bar{x}$ in many of the figures to follow.

The equations of motion for this representation are given, in matrix form, in the Appendix. For this development, a uniform planform, constant stiffness wing was used. A single bending mode, taken to be the deformation shape of a cantilever beam under a uniform distributed load, was chosen to represent wing flexibility. The measure of wing structure bending stiffness is the *in vacuo* cantilevered wing bending frequency, ω_o, expressed in radians/second.

With airspeed, V, held constant, the linearized equations of motion for this model, disturbed from a steady-state equilibrium position, are expressed in matrix form as follows:

$$[s^2[M]+s[B]+[K]]\{\xi\}=\{0\} \tag{1}$$

In this equation, the time-dependent motion is of the form e^{st}, while the complex amplitudes of the pitch, plunge, and bending degrees-of-freedom (or their nondimensional counterparts) form the vector $\{\xi\}$. The mass matrix $[M]$ is real and symmetrical. Bending acceleration is coupled together with both pitch and plunge acceleration. The source of the damping matrix $[B]$ is aerodynamic in origin. All three degrees-of-freedom are coupled through this matrix. The stiffness matrix $[K]$ consists of terms due to wing flexibility and the aerodynamic "stiffness" of both wing and canard. The parameters appearing in Eq. 1 include: wing sweep, wing root position with respect to the aircraft c.g. (shown as z in Fig. 2), canard size and position, and the weight of the wing relative to the weight of the aircraft fuselage. The general form of Eq. 1 remains the same if unsteady flow assumptions are introduced into the problem. However, in that case, the $[B]$ and $[K]$ matrices are functions of reduced frequency, $k=\omega b/V$.

The aeroelastic divergence condition occurs when $s=0$.

$$[K(q)]\{\xi\}=\{0\} \tag{2}$$

Note that the solution to Eq. (2) requires finding values of dynamic pressure q that make $[K]$ singular. Since $[K]$ contains information about the aircraft wing/canard geometry, the expression for the dynamic pressure necessary to cause a divergence instability will involve parameters describing the entire airplane, not just the wing.

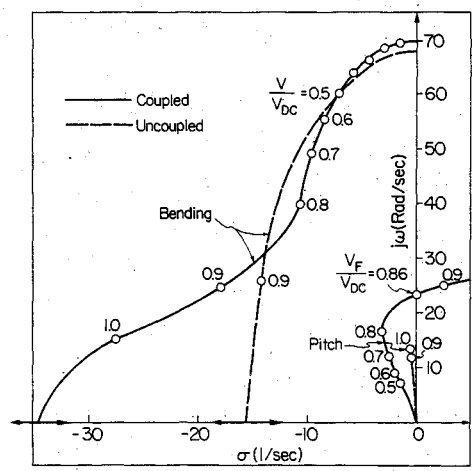

Fig. 3 System eigenvalues as a function of nondimensional airspeed at sea level, V/V_{DC}, for the case 1 aircraft with $\bar{x}=0.45$.

The eigenvalues, s_i of Eq. 1 are functions of airspeed for a fixed altitude and airplane configuration. The system eigenvalues, for a particular value of dynamic pressure, can be real or can occur as complex conjugates of the form

$$s_i=\sigma_i \pm j\omega_i \qquad (j=\sqrt{-1}) \tag{3}$$

These eigenvalues will be displayed in a root-locus or "s-plane" format to enable us to visualize the effects of various parameters on system stability.

The aeroelastic behavior of two FSW airplane configurations will be discussed. The aircraft parameters chosen are within the range of lightweight fighters. Case 1 will illustrate the potential stability behavior of an airplane whose wing is placed in an aft position such that the rigid airplane is statically stable with or without a canard. Case 2 will illustrate the stability behavior of an airplane with a horizontal tail surface. This aircraft configuration may be either stable or unstable without the stabilizer, with the tail supplying additional positive static longitudinal stability.

Case 1—A Stable Wing/Canard Combination

The case 1 airplane has a 30 deg swept forward wing, a wing-mass to fuselage-mass ratio of $\beta=0.11$, and a cantilever wing flexural frequency $\omega_0=68$ rad/s. The quarter-chord root junction is aft of the airplane c.g. at the position $\bar{x}=0.45$. Figure 3 shows system eigenvalues s for increasing values of airspeed V. Airspeed is nondimensionalized with respect to a reference speed, V_{DC}, the airspeed at which this wing would encounter divergence if it were cantilevered at its root.

In Fig. 3, the dashed lines represent the locus of eigenvalues for the uncoupled rigid-body pitching mode (excluding bending and plunge) and the uncoupled wing bending mode (excluding pitch and plunge). The uncoupled pitch mode frequency increases with airspeed; this mode is damped at all airspeeds. Conversely, the bending mode frequency declines with increasing airspeed until its eigenvalue intersects the real axis and then divides. At an airspeed corresponding to V_{DC}, one of these roots enters the right half-plane through the origin. Note that, in the vicinity of $V/V_{DC}=0.90$, the natural frequencies of these two uncoupled modes are nearly identical, indicating the potential for a frequency merging phenomenon. When the coupling terms and the plunge freedom are restored to the equations of motion, the character of the system eigenvalues is far different, as indicated by the solid curves in Fig. 3. The coupled bending mode is well damped at all airspeeds. At $V=V_{DC}$, this mode is still oscillatory. Therefore, the introduction of rigid-body coupling appears to stabilize the coupled bending mode.

The coupled pitch mode frequency and damping increase with increasing airspeed, until a velocity slightly above $V=0.8V_{DC}$ is reached. This pitch root then moves toward the right half-plane as airspeed increases. At $V=0.86V_{DC}$ the pitching mode becomes unstable at a frequency of 23 rad/s. Aeroelastic coupling among the rigid-body modes and the bending mode leads to a dynamic instability of the airplane that will be referred to as "body-freedom flutter."

At the higher frequencies and lower speeds shown in Fig. 3, the reduced frequency is relatively large, leading one to be wary of the quantitative results. However, near the instability speed, reduced frequencies are in the range 0.02-0.03, so that more acceptable accuracy is anticipated. Although the traditional scheme of identifying aeroelastic modes (bending, pitching) has been used here, each mode contains large amounts of bending, plunge, and pitch displacement.

While the inclusion of the aircraft plunge degree-of-freedom is important to the analysis, the two roots corresponding to plunge displacement and plunge velocity are not shown in Fig. 3. The plunge displacement root always lies at the origin of the s-plane, reflecting the fact that our model is really a 5th-order model, since altitude changes produce no forces or moments on the aircraft. The plunge velocity root for this example was found to lie on the negative real axis very near the origin, for all airspeeds investigated.

Figure 4 illustrates the eigenvector associated with the unstable pitch root. Downward plunge is accompanied by nose-up pitch and upward wing bending. These motions are nearly in phase with each other for $\bar{x}=0.45$.

As the cantilever wing divergence speed is approached, aeroelastic forces cause the wing to become more flexible. While downward plunge velocity and nose-up pitch velocity cause wing aerodynamic damping moments that tend to oppose additional pitching motion, the wing bending velocity is in the opposite direction and creates a negative effect. The wing bending velocity causes negative damping moments that overcome damping supplied by the pitch and plunge motion of the aircraft. Thus, wing flexibility leads to a "pitch" instability.

In addition to the body-freedom instability just discussed, an aeroelastic divergence speed occurs at a velocity $V=V_{DA}=2.59\ V_{DC}$. The mode shape for this instability involves upward wing bending and nose-down pitch. This type of instability will be discussed later in the paper.

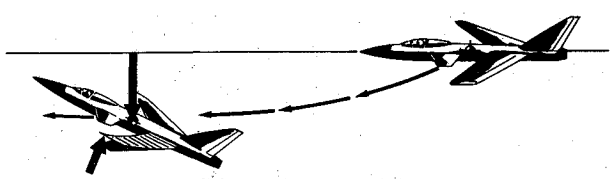

Fig. 4 Body-freedom flutter mode with $\bar{x}=0.45$ and $\Lambda=-30$ deg.

A plot of the eigenvalues for this aircraft when the wing is moved forward to $\bar{x}=0.33$ is shown in Fig. 5. The cantilever wing divergence speed is unchanged. One noticeable difference between Figs. 5 and 3 is that now the "ancestry" of the flutter mode appears to be the wing bending mode. The pitch mode is now stable beyond $V=V_{DC}$. Despite its apparent change of ancestry, the dynamic instability with $\bar{x}=0.33$ still occurs at about the same frequency as that shown in Fig. 3, and still involves substantial coupling among the three degrees-of-freedom. Note also that the body-freedom flutter speed has been increased by decreasing the longitudinal distance between the wing and the aircraft c.g..

With the canard position relative to the aircraft c.g. held fixed, the wing position, $\bar{x}$, was varied to determine its effect upon vehicle aeroelastic stability. Figures 3 and 5 are typical of the two types of eigenvalue behavior observed during these studies. Figure 6 presents a synoptic of the relationship between wing position $\bar{x}$ and the nondimensional flutter speed, V_F/V_{DC}, and flutter frequency, ω_F/ω_0. Also shown on the upper scale in Fig. 6 are values of static margin associated with this example.

In Fig. 6, it is seen that longitudinal movement of the wing toward the aircraft c.g. is associated with an increase in the body-freedom flutter speed. The ratio V_F/V_{DC} actually exceeds unity when the aircraft is statically unstable. These latter values have no significance, however, since the aircraft cannot be flown in a statically unstable regime unless stability augmentation is added. In that case, the present analytical model is no longer valid. Note also that the flutter frequency is in the vicinity of one-third of the in vacuo wing fundamental bending frequency. In addition to the body-freedom instabilities, the aircraft may encounter aircraft aeroelastic divergence. This mode of instability is aperiodic in time, and it is to this potential mode of instability that attention is now turned.

An aperiodic instability occurs if an eigenvalue s is real and greater than zero. This mode of instability is sometimes referred to as "dynamic divergence." It has been characterized by the onset of a looping maneuver in which the increased lift from the flexible wing drives the aircraft upward (or downward) and also increases the pitch attitude. The term dynamic divergence is somewhat tautological. Therefore the term "aircraft aeroelastic divergence" will be used to refer to the static vehicle instability produced by combined rigid-body/flexible-wing displacement.

The presence of aperiodic instabilities may be detected by using Eq. (2) as an eigenvalue problem with q as the unknown parameter. Values of q that cause the matrix $[K]$ to become

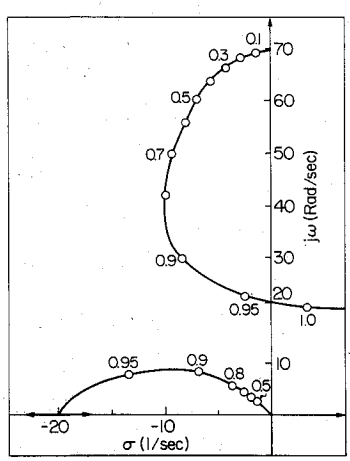

Fig. 5 System eigenvalues for coupled bending and pitching modes as a function of nondimensional airspeed, V/V_{DC}, for the case 1 aircraft with $\bar{x}=0.33$.

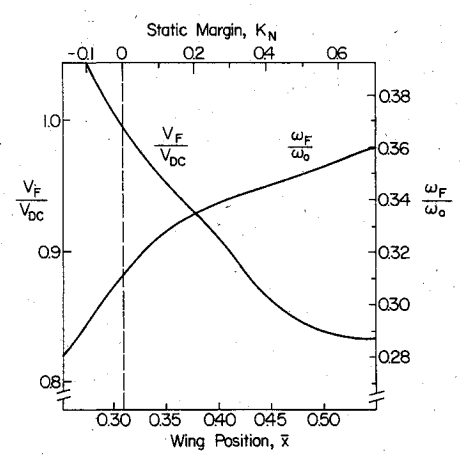

Fig. 6 Nondimensional body-freedom flutter speed V_F/V_{DC} and flutter frequency ω_F/ω_0 vs $\bar{x}$ and static margin K_N, for the case 1 aircraft.

singular correspond to neutral stability speeds for the aircraft. There are three solutions for dynamic pressure that produce neutral stability of this three-degree-of-freedom model.

First of all, the aircraft is neutrally stable in plunge at any airspeed since there are no nonzero terms in the $[K]$ matrix corresponding to the plunge degree-of-freedom. Second, if $q=0$, the aerodynamic pitch stiffness becomes zero and the aircraft is neutrally stable in pitch. Finally, a third root, termed q_{DA}, exists; this corresponds to an aircraft aeroelastic divergence dynamic pressure at airspeed V_{DA}.

The value of the speed V_{DA} in relation to V_{DC}, the cantilever wing divergence speed, is found from the determinant of the stiffness matrix given in the Appendix.

$$\frac{V_{DA}}{V_{DC}}=\left(\frac{5(\bar{y}-\bar{d}\bar{f})}{(\bar{y}-5\bar{d}\bar{f}-0.4\sin\Lambda)}\right)^{1/2} \tag{4}$$

where

$$\bar{y}=\bar{x}+\tfrac{1}{2}\sin\Lambda \tag{5}$$

and

$$\bar{d}\bar{f}=\frac{\bar{d}f}{\cos\Lambda}=\left(\frac{d}{l}\right)\left(\frac{S_c}{S}\right)\left(\frac{C_{L_{\alpha_c}}}{C_{L_\alpha}}\right)\Big/\cos\Lambda \tag{6}$$

$\bar{y}$ is the longitudinal distance (in wing lengths, l) between the airplane c.g. and the rigid wing spanwise center of pressure (CP) at the wing midspan. The numerator of Eq. (4) is a measure of the longitudinal static stability of the rigid aircraft since, for a stable airplane, $(\bar{y}-\bar{d}\bar{f})$ must be greater than zero. Equation (4) indicates that V_{DA} may be substantially different from V_{DC}, depending upon the wing sweep angle and the placement of the wing and stabilizer surfaces with respect to the aircraft c.g. Note also that, consistent with the term "static" instability, no inertia terms appear in Eq. (4).

For the present aircraft configurations, the ratios V_{DA}/V_{DC} and V_F/V_{DC} are plotted vs $\bar{x}$ in Fig. 7. The canard size and position (corresponding to the term $\bar{d}\bar{f}$) are held fixed. Note that, as $\bar{x}$ decreases from a value of 0.55, the aircraft divergence speed increases rapidly until, near $\bar{x}=0.35$, V_{DA} becomes infinite. Further forward movement of the wing root (a decrease in static margin) causes q_{DA} to become negative, so that V_{DA} is imaginary. With a zero static margin, $V_{DA}/V_{DC}=0$. As negative static margin increases, so too does V_{DA}. However, the rigid airplane is now statically unstable, so that the V_{DA}/V_{DC} values to the left of the zero static margin line in Fig. 7 are not attainable.

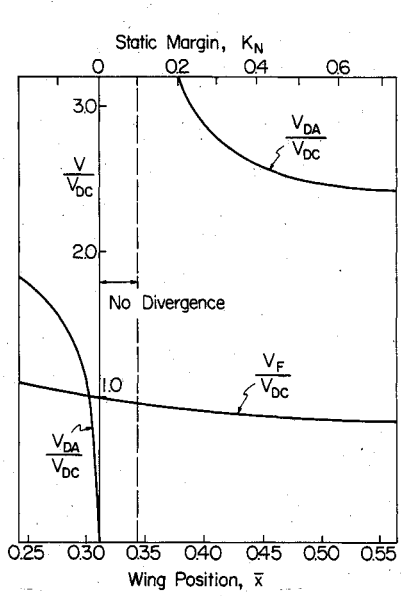

Fig. 7 Nondimensional instability speeds V_F/V_{DC} and V_{DA}/V_{DC} vs $\bar{x}$ and static margin K_N for the case 1 aircraft.

The effects of both wing position and horizontal stabilizer position on aircraft aeroelastic divergence are illustrated in Fig. 8. In this figure the ratio V_{DA}/V_{DC} is plotted against static margin for the 30 deg FSW aircraft with the wing in three different longitudinal positions. Static margin is varied by moving the horizontal stabilizer. Equation (4) indicates that the stabilizer location cannot affect the aircraft divergence speed if $\Lambda=-30$ deg and $\bar{x}=0.30$. This is indicated by the horizontal line in Fig. 8.

If the wing root is placed in the position $\bar{x}=0.35$ and the static margin is then varied by changing the stabilizer position, the aircraft divergence speed will be above V_{DC} if the rigid body-static margin K_N is positive. As K_N tends to infinity, V_{DA} approaches V_{DC}. This occurs because the tail acts as a pitch spring. If the tail lies far enough aft of the c.g., the fuselage is effectively restrained against rotation. The aircraft divergence event closely resembles a cantilever wing phenomenon. As the tail moves closer to the c.g., some aerodynamic load relief, in the form of fuselage pitch, is furnished. This has the effect of increasing the aircraft aeroelastic divergence speed. This effect is similar to that described by Hancock[16] in the case of torsional divergence of an unswept wing.

When the wing root is placed at the $\bar{x}=0.25$ longitudinal position, a tail surface is required for positive static margin. For this case, V_{DA} is below V_{DC} in the range of practical interest, $K_N>0$. The primary source of the divergence instability in this case is the destabilizing aeroelastic effect of the forward CP shift caused by wing bending.

This latter result suggests that, in some cases, aircraft aeroelastic divergence, not flutter, might be the critical mode of instability for the FSW. To examine this possibility, attention will again turn to the dynamic instability problem.

Case 2—Wing/Tail Configuration

Longitudinal stability of the aircraft can be maintained no matter what the wing position $\bar{x}$ may be, provided that the horizontal stabilizer is properly located. In some cases, d must be negative. Figure 9 shows a plot of the eigenvalues for a 30 deg forward swept wing with the horizontal tail positioned at $\bar{d}=-1.5$ and -2.0. For this example the wing root is placed at $\bar{x}=0.30$ so that the aircraft aeroelastic divergence speed is not affected by the tail position. With $\bar{d}=-1.5$, body-freedom flutter occurs before divergence. However, when $\bar{d}=-2.0$, flutter does not occur at all because of the "looping" characteristic of the bending mode eigenvalue.

In Fig. 10, plots of the instability speeds, as a fraction of V_{DC}, are shown vs stabilizer position, for this aircraft with $\bar{x}=0.30$. In the range $-1.80<\bar{d}<0.15$ body-freedom flutter is the critical mode of instability. Outside this range, aircraft divergence appears at a lower speed than flutter. For values of $\bar{d}$ less than -1.95, flutter always appears at a higher, but unattainable, speed. If d is less than -1.15, boty-freedom flutter will not occur at any airspeed.

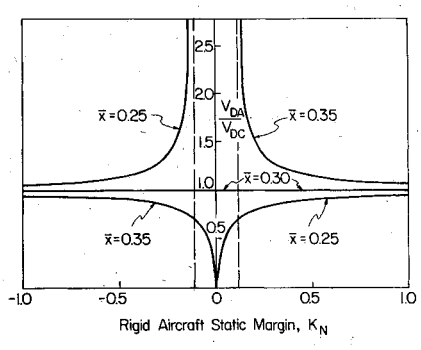

Fig. 8 Nondimensional aircraft divergence speed V_{DA}/V_{DC} vs static margin for three wing positions of the case 1 aircraft.

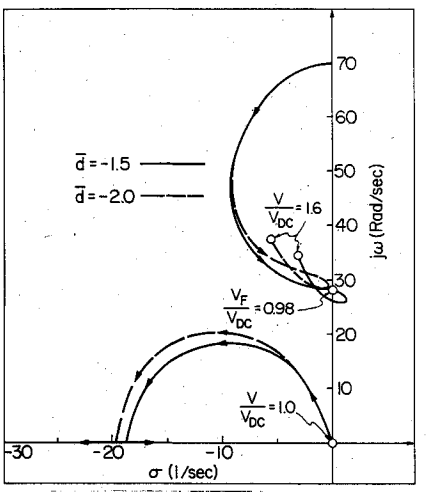

Fig. 9 System eigenvalues for coupled bending and pitching modes as a function of increasing airspeed. Case 2 aircraft with a horizontal tail at two different positions.

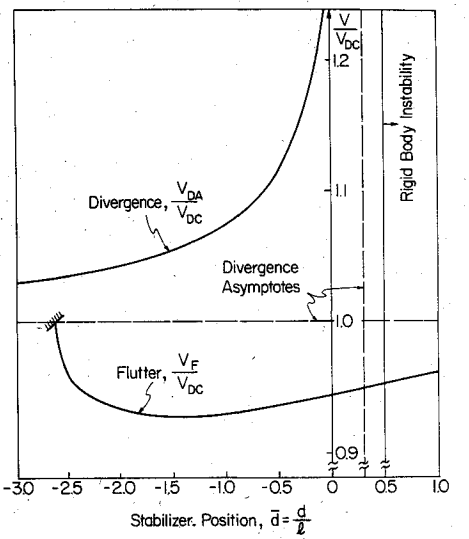

Fig. 12 Effect of horizontal stabilizer position $\bar{d}$ on nondimensional flutter speed and aircraft divergence speed. Case 2 aircraft with $\bar{x}=0.35$.

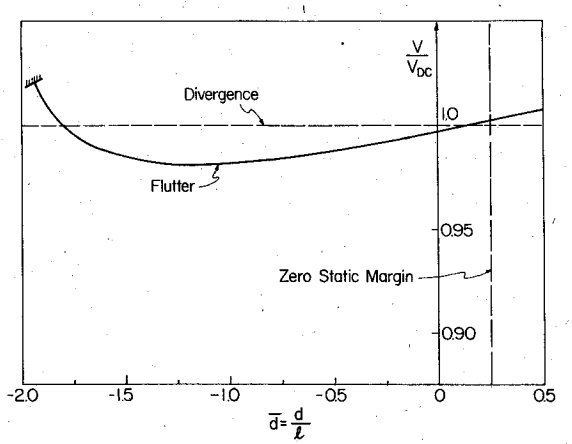

Fig. 10 Effect of horizontal stabilizer postition $\bar{d}$ on nondimensional flutter speed and aircraft divergence speed. Case 2 aircraft with $\bar{x}=0.30$.

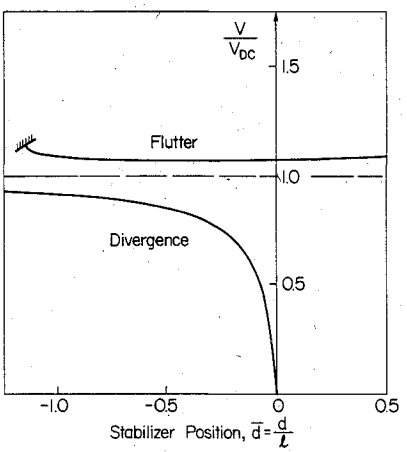

Fig. 11 Effect of horizontal stabilizer position $\bar{d}$ on nondimensional flutter speed and aircraft divergence speed. Case 2 aircraft with $\bar{x}=0.25$.

Similar plots are given in Figs. 11 and 12 for the same configuration, but with the wing root placed in the positions $\bar{x}=0.25$ and $=0.35$, respectively. With the wing root at $\bar{x}=0.25$, a horizontal tail is necessary for longitudinal stability. Figure 11 indicates that aircraft divergence is always the critical mode when $\bar{x}=0.25$. Body-freedom flutter always appears at a higher, but unattainable, speed. If d is less than -1.15, body freedom flutter will not occur at any airspeed.

Figure 12 summarizes the results of the stability analysis of the airplane when the wing root reference point is at $\bar{x}=0.35$. In this case, body-freedom flutter is critical for a range of stabilizer positions $-2.62<\bar{d}\leq 0.5$. Beyond $\bar{d}=-2.62$, flutter does not occur at any airspeed. Aircraft divergence speed declines as the stabilizer moves aft, indicating that an increased pitch stiffening is present.

These latter results indicate that when the wing root is positioned far aft of the c.g., body-freedom flutter is likely to be the critical instability mode; if so, it will appear at an airspeed less than V_{DC}. Moving the wing forward tends to increase the flutter speed and decrease the aircraft divergence speed. For a given aircraft, which of these two instability modes is critical depends upon the stabilizer placement (and size).

Conclusion

The purpose of the idealized FSW aircraft stability examples presented in this paper was to identify potential problem areas related to the dynamic stability of a freely flying, flexible, forward swept wing aircraft. Because of the simplicity of the model and the limited number of examples studied, it is not possible to draw conclusions relevant to all FSW configurations. However, a number of results obtained from these examples are significant.

Because the phenomenon of lifting surface divergence involves a destiffening of an aerodynamic surface, with the potential for generating large aerodynamic forces and moments, the deliterious coupling of a low-frequency elastic mode with FSW aircraft rigid-body modes of motion has been shown to be a very likely possibility. This coupling may lead either to a dynamic instability, termed body-freedom flutter, or to an aperiodic instability called aircraft aeroelastic divergence. The degree of modal interaction depends upon the inertial, aerodynamic, and stiffness characteristics of the aircraft. For the configurations studied, the instability speeds of the freely flying aircraft were close to the clamped wing divergence speed; however, the modes of instability were substantially different from those associated with cantilever wing divergence. The results of these investigations indicate that the location of the horizontal stabilizer and the wing relative to the aircraft c.g. is important to flexible FSW aircraft stability. In particular, the presence of a large tail (or

tail volume) may provide enough aerodynamic pitch stiffness that body-freedom flutter is precluded. However, in that case, aircraft aeroelastic divergence or other conventional flutter phenomena may become active constraints on the flight envelope.

Finally, the results presented in this paper are derived from considerations of attitude stability. The development of the equations of motion has assumed that the perturbations of the aircraft motion from a rectilinear flight path are very small. In this case the axis system used to describe the pitch, plunge and bending displacements is translating with the aircraft at a constant speed and is thus Newtonian. As Milne[17] points out, there is a potential drawback to this approach in that changes in forward speed are excluded. As a result, the possibility of coupling between the short-period mode, as it tends to divergence, and the phugoidal mode is excluded from the present analysis. While such short-period/phugoidal coupling is possible, it has not been observed in any other FSW studies known to the authors. However, the present results do indicate that close attention should be paid to the interactions between traditional rigid-body or zero-frequency modes and structural modes of the vehicle. Therefore, for analysis purposes, it may be wise to investigate the potential for such interaction on an actual flight vehicle that has aircraft aeroelastic divergence as a design constraint.

Acknowledgment

This study was supported by NASA/Langley Research Center Grant NAG-1-157.

Appendix—Equations of Motion

Nomenclature

$\bar{b}$ = b/l

C_{L_α}, $C_{L_{\alpha c}}$ = lift curve slopes for wing and canard, respectively

$\bar{d}$ = d/l

$\bar{f}$ = $\dfrac{(S_c/S)\,(C_{L_{\alpha_c}}/C_{L_\alpha}}{\cos\lambda}$

I_f = fuselage pitch moment of inertia about its c.g.

I_w = wing cross-sectional mass moment of inertia about the y axis

m = wing mass per unit length along spanwise y axis

M_F = fuselage mass

M_T = total aircraft mass

$\bar{r}_0$ = fuselage nondimensional radius of gyration, $=I_f/M_F l^2)^{1/2}$

$\bar{r}_\alpha$ = wing sectional radius of gyration, $=(I_w/ml^2)^{1/2}$

S = planform area of right half of wing

S_c = planform area of right half of canard/tail

$\bar{x}$ = x/l

$\bar{y}$ = $\bar{x}+\frac{1}{2}\sin\Lambda$

$\bar{z}$ = $z/l=\bar{x}+(\bar{b}/2)\cos\Lambda$

β = $2ml/M_F$

μ = $\pi\rho Sb/M_T$

ρ = air density

This Appendix presents the equations of motion used to describe the three-degree-of-freedom forward swept wing aircraft. The definition of geometrical parameters used in this development is presented in Fig. 2. Degrees of freedom are: w, aircraft plunge, positive downward; θ, aircraft pitch attitude, positive nose-up; and h, wing bending deformation, positive downward. The equations of motion were developed using Lagrange's equations, together with an assumed deflection shape for a single wing bending vibration mode.

Table A Parameter values for this study

$l=15$ ft.	$\beta=0.11$
$M_T/2S=3.8$	$\bar{r}_0=0.61$
$\bar{r}_\alpha=0.0$	$\bar{f}=0.17$
$\omega_0=68$ rad/s	$\bar{b}=0.1453$

The analysis is restricted to a uniform planform wing with its mass distributed uniformly along and about the y axis located at the wing midchord. The mass matrix was developed by assuming a mode shape for flexure, $h(y,t)$, relative to the effective root. The wing flexure is given in terms of wing tip deflection, $\bar{h}(t)$.

$$h(y,t)=\bar{h}(t)\gamma(y) \tag{A1}$$

where

$$\gamma(y)=\tfrac{1}{3}[6(y/l)^2+4(y/l)^3+(y/l)^4] \tag{A2}$$

The mass matrix is then calculated from a kinetic energy expression that includes the inertia of the wings and fuselage.

The structural stiffness of the wing is developed from an expression for U, the bending strain energy of the wing. Wing strain energy may be expressed in terms of the *in vacuo* cantilever natural frequency ω_0 as:

$$U=2\left[\frac{I}{2}m\omega_0^2\int_0^l\gamma^2\mathrm{d}y\right]\bar{h}^2 \tag{A3}$$

The aerodynamic forces acting upon the aircraft wings and the canard are deformation dependent. Although the flow was assumed to be quasi-steady ($k=0$), two-dimensional unsteady strip theory (see Ref. 18) was used to develop expressions for the distributed wing lift and pitching moment. The principle of virtual work was used to develop the generalized forces necessary for Lagrange's equations. The line of aerodynamic centers is assumed to be at the ¼-chord position in this formulation. Thus ratios of V_F/V_{DC} shown in the main body of the paper are strictly valid only for subsonic flow. In keeping with quasi-steady assumptions, the Theodorsen circulation function, $C(k)=F(k)+iG(k)$ was set equal to unity, i.e. $F(k)=1$ and $G(k)=0$.

The aircraft plunge and wing tip displacements have been normalized with respect to the wing span dimension, l, so that a new set of coordinates $\{\bar{\xi}_i\}$ are defined as follows:

$$\begin{Bmatrix}\bar{\xi}_1\\ \bar{\xi}_2\\ \bar{\xi}_3\end{Bmatrix}=\begin{bmatrix}1/l & 0 & 0\\ 0 & 1/l & 0\\ 0 & 0 & 1\end{bmatrix}\begin{Bmatrix}w\\ \bar{h}\\ \theta\end{Bmatrix} \tag{A4}$$

In terms of the nondimensional coordinates in Eq. (A4), the matrices in Eq. (1) are given below, with the following definitions of additional parameters:

$$D=\rho VSC_{L_\alpha}\cos\Lambda/M_T \tag{A5}$$

$$Q=\rho V^2SC_{L_\alpha}\cos^2\Lambda/M_T l \tag{A6}$$

The mass matrix $[M]$ is composed of two parts, that due to aircraft mass and that due to apparent mass of the fluid surrounding the wing. The mass matrix may be written as:

$$[M]=[M^{(1)}+\mu[M^{(2)}] \tag{A7}$$

The matrices in Eq. (A7) are defined in Eqs. (A8) and (A9).

$$[M^{(1)}] = \begin{bmatrix} 1 & \frac{2}{5}\left(\frac{\beta}{1+\beta}\right) & 0 \\ & \frac{104}{405}\left(\frac{\beta}{1+\beta}\right) & \left(\frac{\beta}{1+\beta}\right)\left(\frac{2}{5}\bar{z}+\frac{13}{45}\sin\Lambda\right) \\ \text{Symmetric} & & \frac{\bar{r}_0^2}{(1+\beta)^2}+\beta(\bar{z}+\tfrac{1}{2}\sin\Lambda)^2 \\ & & \left(\frac{\beta}{1+\beta}\right)\left(\frac{1}{12}\sin^2\Lambda+\bar{r}_\alpha^2\cos^2\Lambda\right) \end{bmatrix} \tag{A8}$$

$$[M^{(2)}] = \begin{bmatrix} 1 & \frac{2}{5} & \bar{y}+\tfrac{1}{2}\bar{b}\cos\Lambda \\ & \frac{104}{405} & \bar{y}+\frac{2}{9}\sin\Lambda+\frac{\bar{b}}{2}\cos\Lambda \\ \text{Symmetric} & & \bar{y}^2+\frac{1}{12}\sin^2\Lambda+\bar{y}\frac{\bar{b}}{2}\cos\Lambda \\ & & +\frac{3}{8}\bar{b}^2\cos^2\Lambda \end{bmatrix} \tag{A9}$$

The aerodynamic damping matrix is written as:

$$[B] = D[\bar{B}] \tag{A10}$$

where $[B] =$

$$\begin{bmatrix} 1+\bar{f} & \frac{\bar{b}}{2}\tan\Lambda+\frac{2}{5} & \bar{y}+\bar{b}(\tfrac{1}{2}+\cos\Lambda)-\bar{f}\bar{d} \\ \frac{2}{5} & \frac{\bar{b}}{4}\tan\Lambda+\frac{104}{405} & \frac{\bar{b}}{5\cos\Lambda}+\frac{2}{5}\left(\bar{y}+\frac{2}{9}\sin\Lambda+\bar{b}\cos\Lambda\right) \\ \bar{y}-\bar{f}\bar{d} & \frac{\bar{b}}{2}\left(\bar{y}+\frac{\sin\Lambda}{10}\right)\tan\Lambda & \frac{\bar{b}\bar{y}}{2\cos\Lambda}-\frac{\bar{b}^2}{2}\sin^2\Lambda \\ & +\frac{2}{5}\left(\bar{y}+\frac{2}{9}\sin\Lambda\right) & +\left(\bar{y}^2+\frac{\sin^2\Lambda}{12}+\bar{b}\bar{y}\cos\Lambda\right) \\ & +\frac{\bar{b}^2}{4}\sin\Lambda & +\bar{f}\bar{d}^2 \end{bmatrix} \tag{A11}$$

The combination of aerodynamic stiffness and wing structural stiffness provides the terms in the $[K]$ matrix.

$$[K] = \begin{bmatrix} 0 & Q\tan\Lambda & \frac{Q}{\cos\Lambda}+\frac{\bar{f}}{\cos\Lambda} \\ 0 & \frac{Q}{2}\tan\Lambda \\ & +\omega_0^2\left(\frac{\beta}{1+\beta}\right)\left(\frac{104}{405}\right) & \frac{2}{5}\frac{Q}{\cos\Lambda} \\ 0 & Q\tan\Lambda\left(\bar{y}+\frac{\sin\Lambda}{10}\right) & \frac{Q\bar{y}}{\cos\Lambda}-\frac{\bar{f}\bar{d}}{\cos\Lambda} \end{bmatrix} \tag{A12}$$

A number of parameters used to compute matrices appearing in Eqs. A8-A12 were held fixed throughout the study. They are given in Table A1.

References

[1] Krone, N.J. Jr., "Divergence Elimination with Advanced Composites," AIAA Paper 75-1009, Aug. 1975.

[2] Krone, N.J. Jr., "Forward Swept Wing Flight Demonstrator," AIAA Paper 80-1882, Aug. 1980.

[3] Miller, G.D., Wykes, J.H., and Brosnan, M.J., "Rigid Body-Structural Mode Coupling on a Forward Swept Wing Aircraft," AIAA Paper 82-0683, May 1982.

[4] Weisshaar, T.A., "Divergence Suppression of Forward Swept Wings", Virginia Polytechnic Institute and State University, Beacksburg, Va., Final Report NASA Grant, NASI-15080-Task No. 16, Sept. 1980.

[5] Weisshaar, T.A., Zeiler, T.A., Hertz, T.J., and Shirk, M.H., "Flutter of Forward Swept Wings, Analyses and Tests," AIAA Paper 82-0646, May 1982.

[6] Frazer, R.A. and Duncan, W.J., "Wing Flutter as Influenced by the Mobility of the Fuselage," British Aeronautical Research Council, R.&M. 1207, 1929.

[7] Schwendler, R.G., and Hill, J.H., "Low Frequency Instabilities of Free Systems," AFFDL, Wright-Patterson AFB, Ohio, Rept. ASD-TDR-63-655, Nov. 1963.

[8] Gaukroger, D.R., "Wind Tunnel Test on Model Delta Wing Under Fixed and Free-Root Conditions," British Aeronautical Research Council, R.&M. 2826, 1955.

[9] Gaukroger, D.R., "Wind Tunnel Test on the Symmetric and Antisymmetric Flutter of Sweptback Wings," British Aeronautical Research Council, R.&M. 2911, 1955.

[10] Gaukroger, D.R., "Wing Flutter," *AGARD Manual on Aeroelasticity,* Part V, 1960, Chap. 2.

[11] Cunningham, H.J. and Lundstrom, R.R., "Description and Analysis of a Rocket-Vehicle Experiment on Flutter Involving Wing Deformation and Body Motions," NACA TN 3311, Jan. 1955.

[12] Weisshaar, T.A. and Ashley, H., "Static Aeroelasticity and the Flying Wing, Revisited," *Journal of Aircraft,* Vol. 11, Nov. 1974, pp. 718-728.

[13] Jones, R.T. and Nisbet, J.W., "Aeroelastic Stability and Control of an Oblique Wing," *The Journal of the Royal Aeronautical Society,* Vol. 80, Aug. 1976, pp. 365-369.

[14] Weisshaar, T.A., and Crittenden, J.B., "Flutter of Asymmetrically Swept Wings," *AIAA Journal,* Vol. 14, Aug. 1976, pp. 993-994.

[15] Crittenden, J.B., Weisshaar, T.A., Johnson, E.H., and Rutkowski, M.J., "Aeroelastic Stability Characteristics of an Oblique Winged Aircraft," *Journal of Aircraft,* Vol. 15, July 1978, pp. 429-434.

[16] Hancock, G.J., "The Static Aeroelastic Deformation of Slender Configurations, Part III: Static Stability," *The Aeronautical Quarterly,* Vol. XIV, Feb. 1963, pp. 75-104.

[17] Milne, R.D., "Dynamics of Deformable Airplanes," British Aeronautical Research Council, R.&M. No. 3345, Sept. 1962.

[18] Bisplinghoff, R.L., Ashley, H., and Halfman, R.H., *Aeroelasticity,* Addison-Wesley, Reading, Mass., pp. 394-400.